Research Square

Preprints are preliminary reports that have not undergone peer review.
They should not be considered conclusive, used to inform clinical practice,
or referenced by the media as validated information.

Long-term geomorphic evolution of an inactive Tailings Storage Facility in a dynamic landscape

Saraswati Thapa

Saraswati.Thapa@ed.ac.uk

University of Edinburgh

Thomas Coulthard

Manchester Metropolitan University

Richard D. Williams

Earth Sciences New Zealand

Grigorios Vasilopoulos

University of Hull

Patrick Byrne

Liverpool John Moores University

Karen Hudson-Edward

University of Exeter

Decibel V. Faustino-Eslava

University of the Philippines Los Baños

Eduardo Calzeta

University of the Philippines Los Baños

Research Article

Keywords:

Posted Date: November 25th, 2026

DOI: https://doi.org/10.21203/rs.3.rs-11628275/v1

License: This work is licensed under a Creative Commons Attribution 4.0 International License.
Read Full License

Additional Declarations: No competing interests reported.

Long-term geomorphic evolution of an inactive Tailings Storage Facility in a dynamic landscape

Saraswati Thapa*[1,2], Thomas Coulthard[2,3], Richard D. Williams[4,5], Grigorios Vasilopoulos[2], Patrick Byrne [6], Karen Hudson-Edward[7], Decibel V. Faustino-Eslava[8], and Eduardo Calzeta[8]

[1]School of Geosciences, University of Edinburgh, UK
[2]Energy and Environment Institute, University of Hull, UK
[3]Department of Natural Sciences, Manchester Metropolitan University, UK
[4]Earth Sciences New Zealand, NZ
[5]School of Geographical and Earth Sciences, University of Glasgow, UK
[6]Liverpool John Moores University, Liverpool, UK
[7]University of Exeter, UK
[8]School of Environmental Science and Management, University of the Philippines Los Baños, Philippines

Abstract

Tailings storage facilities (TSFs) are major anthropogenic landforms that can significantly alter river dynamics and pose long-term environmental risks if left unmanaged. While abrupt TSF failures have been widely studied, the longer-term degradation and geomorphic adjustment of inactive TSFs remain poorly understood, particularly where these processes are driven by rainfall, water accumulation, sediment infilling, overtopping, dam erodibility, and limited post-closure management. This study investigates Liang cross-valley TSF in Benguet, northern Philippines, which has remained inactive since 1998 but continues to undergo sediment infilling, overtopping, and erosion. The CAESAR-Lisflood landscape evolution model was used to simulate centennial- to millennial-scale geomorphic evolution under observed rainfall conditions. The results showed that progressive sediment infill reduces dam storage capacity, increases overtopping frequency, and accelerates spillway incision and dam-wall erosion, leading to sustained downstream sediment redistribution. Sensitivity analyses revealed that long-term sediment transport and morphological adjustment are more strongly controlled by dam material erodibility than by critical erosion thresholds. Even in low to moderate dam bedrock erosion scenarios, substantial sediment volumes released downstream (> 2 Mm^3 in 10 years; > 3 Mm^3 in 100 years; up to 120–147 Mm^3 in 1,000 years), demonstrating that inactive TSF landforms can remain geomorphically dynamic long after mine closure. These findings highlight often underappreciated gradual TSF failure pathways and the persistent geomorphic hazards underscoring the need for sustained post-closure monitoring and adaptive management.

Keywords: Sediment transport; Geomorphology; Philippines; Modelling; CAESAR-Lisflood

*Corresponding author: Saraswati.thapa@ed.ac.uk

1 Introduction

Metal mining activities can alter geomorphic processes within river catchments through modification of hillslope–channel connectivity, changes in sediment flux, and long-term landscape adjustment (Dethier et al., 2022; Hudson-Edwards et al., 2024, 2011; Macklin et al., 2006; Macklin et al., 2023). In particular, the discharge or release of mine tailings has been shown to generate short- and long-term impacts on fluvial geomorphic dynamics, ecosystems, and humans (Hudson-Edwards et al., 2024, 2011). Tailings are slurries consisting of fine sediment particles ($< \sim$2 mm), water and processing chemicals that remain after the valuable components are removed from ores (Hudson-Edwards et al., 2024; Kossoff et al., 2014). Approximately 7 to 13 billion tonnes of tailings are produced worldwide each year (Hancock and Coulthard, 2022; Hudson-Edwards et al., 2024, 2011; Mudd and Boger, 2013). In contemporary large-scale operations, tailings are stored in tailings storage facilities (TSFs), which function as large anthropogenic geomorphic landforms embedded within existing drainage networks. Approximately 25,000 active, inactive, closed, or abandoned TSFs have been mapped globally, and of these around 3,400 are currently active (Hudson-Edwards et al., 2024; Macklin et al., 2023). As a result, TSFs are not only engineered containment systems, but also long-lived anthropogenic landforms capable of influencing catchment-scale geomorphic dynamics through time.

Methods of TSF construction are highly variable (Hudson-Edwards et al., 2024), but three broad designs predominate. Ring-dike TSFs are commonly built on relatively flat terrains and are enclosed by embankments, also referred to as dams, on all sides. In contrast, side-hill and cross-valley TSFs are more common in mountainous settings, where storage is partly controlled by natural topography. In side-hill TSFs, the facility is built against one valley side and bounded by embankments on the open margins, whereas in cross-valley TSFs an embankment is constructed across the valley floor and the adjoining valley walls provide lateral confinement (Dong et al., 2020; Hancock, 2021; Slingerland et al., 2022; World Bank, 2019). TSF embankments are generally constructed from waste rock, borrowed earth materials, and other coarse fill available on site; in some cases, suitably coarse fractions of tailings may also be used depending on the construction method and local conditions.

In the last 100 years, 1.2% of TSFs have failed worldwide, a rate much higher than that of dams constructed to store water that have failed (Azam and Li, 2010; Domingo et al., 2024). Since the 1960s alone, more than 350 TSFs failures have been recorded worldwide (https://www.wise-uranium.org/mdaf.html). These failures can result in loss of life, ecosystem degradation, damage to infrastructure and livelihoods, and contamination of water and sediment with potentially toxic metal(loid)s such as As, Cd, Cu, Hg, Pb, Sb, and Zn. They often require extensive remediation, long-term management, and costly recovery efforts (Azam and Li, 2010; Eriksson and Adamek, 2016; Foundation, 2003; Kossoff et al., 2014). Despite growing research on TSF failures,(Armstrong et al., 2019; Hudson-Edwards et al., 2024, 2011; Kossoff et al., 2014; Mahdi et al., 2020; Zhao et al., 2026), two important limitations persist. First, most studies focus on geomorphic change following sudden catastrophic dam breaches, whereas relatively few examine the longer-term geomorphic responses that drive progressive degradation over decadal to millennial timescales (Dong et al., 2020; Hudson-Edwards et al., 2011; Liu et al., 2026). This is important because TSFs do not always fail through a single abrupt collapse but instead can degrade progressively through processes such as sediment infilling, overtopping, incision, and wall erosion. Over time, these processes can reduce storage capacity, weaken structural stability, and sustain downstream sediment release even without a catastrophic breach. Focusing only on catastrophic failures therefore risks underestimating long-term geomorphic hazards. Second, research has tended to concentrate on active or recently decommissioned facilities, while numerous abandoned TSFs that remain unmanaged for decades to centuries are poorly understood. This matters because once monitoring and maintenance cease, these landforms continue to interact with catchment hydrology and geomorphic

processes, potentially creating persistent and unrecognised risks to downstream environments and communities. Such risks are likely to be especially acute in dynamic mountain settings, where intense rainfall and high erosion rates can accelerate post-closure change.

Among TSF types, cross-valley facilities are particularly important because they are embedded directly within drainage networks and therefore intercept runoff and sediment transport from the upstream catchment. This makes them especially susceptible to progressive infilling, overtopping, spillway incision, and sustained downstream sediment transfer through time. Their post-closure evolution is also highly sensitive to catchment-scale rainfall, runoff, and sediment supply, including material derived from unstable upstream slopes, disturbed mine surfaces, and other legacy mining features. Their strong coupling with catchment hydrology, hydraulic connectivity, and geomorphic processes makes them especially suitable for investigating long-term post-closure geomorphic evolution and gradual failure over decadal to millennial timescales. More broadly, Hudson-Edwards et al., 2024 emphasised that TSF failures should be understood within a catchment and disaster-risk framework, because construction type, storage setting, and landscape connectivity influence both failure pathways and downstream impacts. Several severe TSF disasters have occurred in cross-valley settings, including the 1985 Stava failure in Italy and the 2015 Fundão and the 2019 Brumadinho failures in Brazil (Chandler and Tosatti, 1995; Hudson-Edwards et al., 2024), demonstrating the potentially far-reaching consequences of failure in such environments. Given that cross-valley TSFs can persist as anthropogenic landforms for centuries to millennia, several critical questions remain: (1) how do gradual geomorphic processes control the long-term, decadal to millennial-scale morphological evolution and stability of TSFs? (2) what mechanisms and timescales characterise slow failure processes of TSFs, such as progressive infilling and overtopping? (3) what factors control the longevity of cross valley-fill TSFs? and (4) how much water and sediment may be released downstream from the wider catchment and the TSF area as a result of gradual erosion? This study addresses these questions by focusing on the Liang TSF in the steep Ambalanga catchment in the northern Philippines, which is particularly relevant because its cross-valley configuration, abandonment since 1998, and recent typhoon-related disturbances, which demonstrate that geomorphic instability and associated downstream risks can persist long after mine closure under sustained high-rainfall conditions.

We use the long-term landscape evolution model CAESAR-Lisflood (Coulthard et al., 2013) to simulate up to 1,000 years of geomorphic evolution under observed rainfall conditions to provide a novel process-based framework for assessing the long-term geomorphic risks associated with valley-fill TSFs in mountain environments, including progressive geomorphic degradation, downstream flooding and sediment release, and potential implications for contamination and environmental health.

2 Study area

The Philippines, an archipelagic nation in Southeast Asia, comprises more than 7,500 islands grouped into three main geographic regions: Luzon, Visayas, and Mindanao. The country is characterised by a diverse landscape shaped by active tectonics and a tropical climate, and is exposed to an average of 20 tropical cyclones each year (DOST-PAGASA, 2023). These conditions create a highly dynamic geomorphic environment in which intense storm events frequently trigger slope failures and rapid downstream sediment transport (Panici et al., 2024) . National-scale analysis has shown that Philippine River catchments exhibit substantial topographic diversity, with average catchment slopes ranging from 3.1^o to 28.1^o and average stream slopes from 0.004 to 0.107 m/m (Boothroyd et al., 2025, 2023). This variability highlights the importance of place-based analyses for understanding the geomorphic sensitivity of individual basins. The Philippines is also recognised for its abundant reserves of gold, copper, and nickel, ranking as the fifth most mineral-rich nation in the world. It holds the third, fourth and fifth

largest global gold, copper and nickel reserves, respectively (Reyes et al., 2023). The country has a long history of metal mining, first officially recorded in the mid-16th century when Spanish colonisers conducted alluvial gold mining, followed by copper mining in Panay Island and Benguet Province during the 18th century (Domingo, 1993). After the Philippine government lifted the open-pit mining ban of 2017 in December 2021, mining activities for copper, gold, silver, and complex ores rapidly resumed throughout the country, prompting many companies to increase their production and infrastructure and expand their TSFs (Domingo et al., 2024; Reyes et al., 2023). In the Philippines, the Mines and Geosciences Bureau has identified at least 27 abandoned and inactive mines, underscoring the extent of legacy mining infrastructure and the significance of abandoned TSFs as long-term hazards in steep, typhoon-prone catchments (Aggangan et al., 2019; Jessie et al., 2020).

This study focuses on the Antamok mine area (Figure 1), covering approximately 5.24 km^2 and located in the Ambalanga catchment (88 km^2), Itogon Municipality, within the Baguio gold district, Benguet Province, Luzon island. The area was selected because it represents a well-defined legacy mining landscape with inactive tailings storage infrastructure, a long history of large-scale mine extraction, and documented post-closure geomorphic instability within a steep, typhoon-affected tropical catchment. The Liang River, which drains the Antamok mine area, is a tributary of the Ambalanga River, which flows into the Agno River. The Ambalanga catchment is also referred to as Itogon because it lies within the Itogon municipality (e.g., Corpus et al., 2011; Macasieb et al., 2021; Panici et al., 2024). Throughout this paper, the following naming conventions are used: Itogon refers to the municipality; Ambalanga refers to the river and catchment; Liang River refers to the study tributary; and Antamok refers to the mine site.

The Antamok open pit mine is the first industrialised gold mine in the Philippines (Chaloping-March, 2017; Domingo, 1993; Mines and Geosciences Bureau, US Geological Survey), opened in 1903. In the 1980s, Benguet Corporation reached its operational peak, running five major mines across the Philippines, of which the Baguio-Antamok Gold Operation (BAGO) represented its major gold mining activities in Benguet Province. Widespread regulation of large-scale extraction was introduced in the Philippines in 1984, coinciding with the development of TSFs in the Ambalanga catchment (Domingo et al., 2024; Benguet Corporation, 2026).

Since the closure of the Antamok mine in 1998, monitoring and maintenance of the Liang TSF has been limited, with several recorded incidents of mine tailings release (Cultural Survival, 2023). The vulnerability of long run TSFs in the Philippines has been starkly highlighted by frequent extreme rainfall and typhoon events. For example, the August 2012 Padcal mine tailings breach released approximately 20.6 million tonnes of tailings into the Balog River, affecting about 2.5 km of channel before discharging into the Agno River and reaching San Roque Dam (WISE Uranium Project, 2025). Within the Ambalanga catchment, the Liang TSF presents a comparable vulnerability. Among the four TSFs identified in the catchment(Domingo et al., 2024), the Liang TSF is a cross-valley facility constructed by Benguet Corporation in the 1980s, as part of the corporation's transition from underground extraction to open-pit bulk mining following the depletion of high-grade ore reserves. The TSF spans a steep and narrow valley, standing approximately 90 m high and 450 m wide at the crest, based on measurements derived from satellite imagery and IfSAR DEM, and impounds approximately 9 Mt of fine-grained, sulphur-rich tailings. The facility blocks and traps sediment from a major tributary of the Ambalanga River and occupies a region characterised by intense monsoonal rainfall, frequent typhoons, and elevated landslide risk (Panici et al., 2024).

On 27 October 2016, Typhoon Lawin triggered intense rainfall, which led to a significant tailings leakage from the Liang TSF. More than 50,000 tonnes of tailings flowed through an underground drainage tunnel into the Liang River and were subsequently transported downstream via the Ambalanga River to the Agno River (WISE Uranium Project, 2025; Zhen et al., 2021). Following the event, the Itogon Municipal Council issued a resolution calling for a full

investigation into the cause of the leak and surface tension cracks observed on the Antamok open pit mining TSF wall. The resolution also urged complete rehabilitation of the TSF and the pit at Benguet Corporation's expense (Chaloping-March, 2017). Meanwhile, Benguet Corporation reported that clean-up and containment efforts were initiated in coordination with the Mines and Geosciences Bureau (MGB), the Environmental Management Bureau (EMB), Local Government Units (LGUs) and local communities (Philippine Securities and Exchange Commission (Chaloping-March, 2017; Philippine Securities and Exchange Commission (PSEC), 2016). However, the different accounts between the local council and the company highlighted the lack of alignment between corporate and community responses to legacy mining hazards (Chaloping-March, 2017).

In mid-September 2018, Typhoon Mangkhut (locally known as Ompong) triggered widespread landslides, mud flows and debris flows across northern Luzon (Abancó et al., 2021; Guardian, 2018). Abancó et al. (2021) mapped a total of 1,101 landslides across a 570 km^2 area of the Itogon region, with a fatal landslide in Itogon burying a mining camp and resulting in over 100 fatalities (Guardian, 2018). The event is directly relevant to this study as it triggered debris flows within the Antamok sub-catchment, reduced the storage capacity of the Liang tailings storage facility by approximately 8%, from 3.51 to 3.23 ha (Figure 2), and caused significant downstream sediment redistribution (Panici et al., 2024). The event collectively demonstrates the acute vulnerability of the Liang TSF to extreme rainfall in this region and highlights the importance of understanding how geomorphic processes evolve over longer timescales under repeated climatic forcing, which is the central focus of this study. The 2018 event is also used here for model calibration. The Ambalanga catchment (Figure 1) has a relief of 940 m, with a maximum elevation of 1580 m a.s.l., mean slope of 30° and average stream slope of 16°. The Liang/Antamok River is a tributary of the Ambalanga, which flows into the Agno River (Figure 1). Rivers in the Ambalanga catchment have predominantly mixed sand-gravel beds. The catchment receives a mean annual rainfall of 2200 mm (1998-2015), occurring mainly in the wet season (Domingo et al., 2024). The hydrological and topographic vulnerability of the catchment, combined with aging TSF infrastructure, underscores the urgency of risk assessments and rehabilitation planning to ensure long-term stability in post-closure mining landscapes such as the Liang/Antamok River catchment.

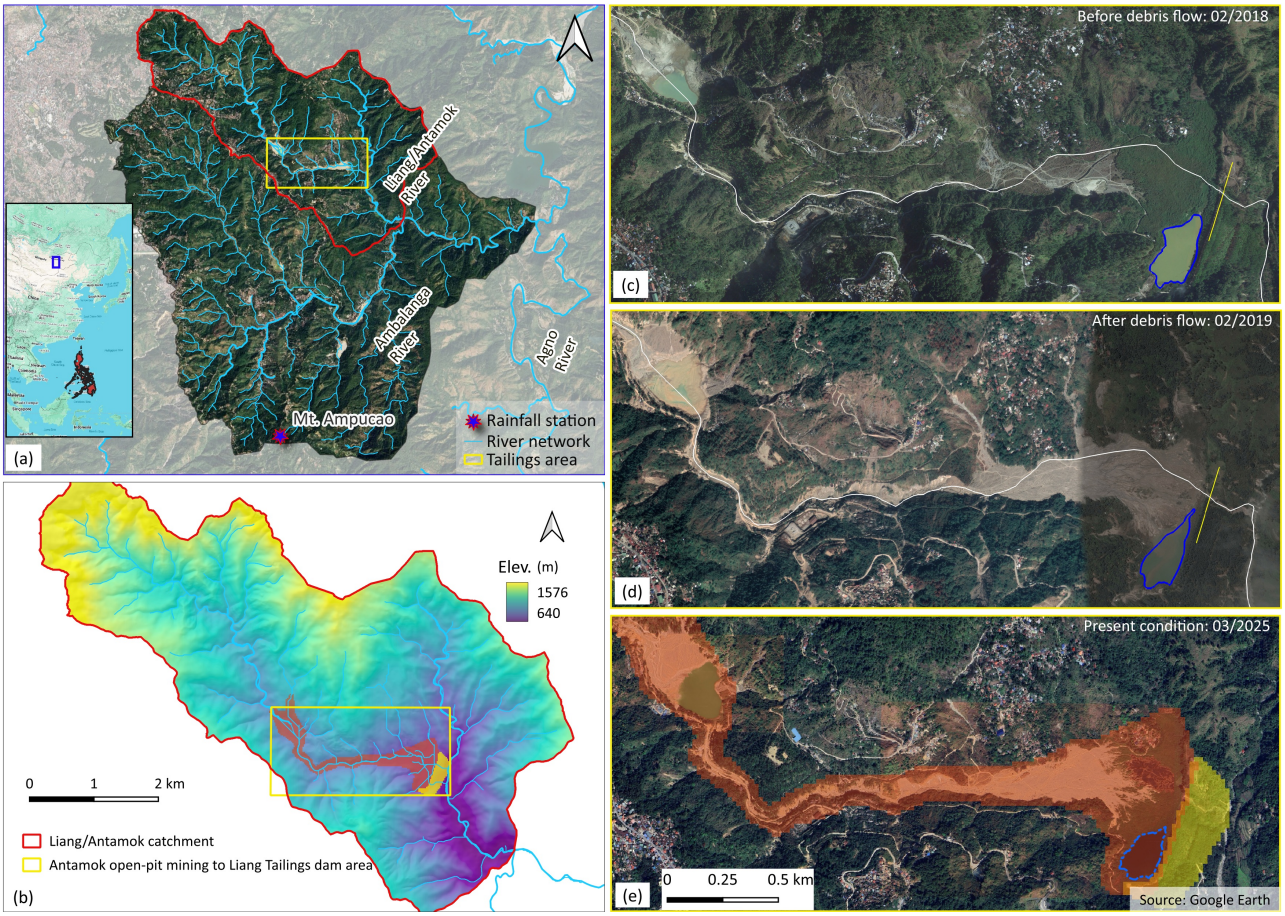

Figure 1: Study area overview and temporal changes in the tailings storage facility site affected by the 2018 debris flow event: (a) Ambalanga basin with the Liang/Antamok sub-catchment marked by a red line polygon with drainage networks produced using a 2013 IfSAR DEM (Grafil and Castro, 2014), the area from the Antamok open-pit mining to downstream dam marked by yellow rectangular box, and a regional rainfall station (Mt. Ampucao) used in the study; Note that the Liang River drains the Antamok sub-catchment as a tributary of the Ambalanga River (see Section 2 for naming conventions used in this study); (b) Elevation map of the model domain derived from the 2013 IfSAR DEM, with shaded polygons indicating areas for sediment tracing from open-pit mining to the dam (red) and for testing impact of variable erosion parameters within the dam area (yellow); (c) Satellite image prior to the debris flow (February 2018), showing intact tailings storage areas; (d) Post-event satellite image (February 2019), illustrating extensive sediment deposition and reduced tailings storage facility storage following the Typhoon Mangkhut-triggered debris flow, with reduced surface water extent (blue polygon), river center (white solid line), and dam top edge (yellow line); and (e) Satellite image of present-day condition of TSF (March 2025), showing partial recovery and vegetation regrowth, dam body (yellow shaded area), and the sediment-tracing zone from the Antamok open-pit mine to the Liang TSF (red shaded area). The sediment transport from the mining area (red polygon) and the rest of the catchment was traced in each simulation to quantify the ratio of sediment outflow from the open-pit mining area (red polygon in Figures 1b and 1e) relative to the rest of the catchment.

3 Methodology

3.1 Model Framework: CAESAR-Lisflood

Several studies have used computer-based models to simulate how TSF might evolve and potentially fail, either suddenly or over time, using both small-scale laboratory experiments and theoretical scenarios (Hancock and Coulthard, 2022; Slingerland et al., 2018a, 2019, 2022; Slingerland et al., 2018b; Thomson and Chandler, 2019). These models predict dam erosion rates, identify weak points, and evaluate the robustness of dam design. However, most of these previous studies are based on hypothetical examples of TSFs and the simulated results are hard to generalise to environments with climatic conditions, landscapes, and dam materials that are substantially different from the assumptions that underpin the hypothetical examples.

This study uses the CAESAR-Lisflood(CL)[1] model to simulate the long-term evolution of the Liang cross valley TSF. The model integrates TOPMODEL for hydrological simulation, LISFLOOD-FP for two-dimensional hydrodynamic flow routing (Bates et al., 2010; Coulthard et al., 2013), and an active-layer approach for sediment erosion, transport and deposition. CL is a physics-based landscape evolution model (LEM) capable of simulating geomorphic change over timescales ranging from individual storm events to millennia, making it well suited to long-term landform stability assessment. CL has previously been applied to assess the long-term geomorphic stability of rehabilitated mine landforms (for example: the Ranger Uranium Mine, Australia (Lowry et al., 2013; Saynor et al., 2019)). Critically, and of direct relevance to this study, CL has also been used to simulate TSF failure scenarios — including progressive overtopping, spillway incision, and loss of containment — for both idealised and design-specific valley-fill TSF configurations (Hancock and Coulthard, 2022; Slingerland et al., 2022; Thomson and Chandler, 2019). These applications demonstrate that CL can reliably reproduce observed geomorphic change in mine-affected catchments and capture the onset of failure pathways, providing confidence in its use for the longer-term projections presented here. This study applies CL for the first time to a real-world abandoned valley-fill TSF in a dynamic environment, using an observed rainfall record and high-resolution topographic data specific to the Liang catchment, northern Philippines.

3.2 Model Inputs and Setup

The model inputs include hourly observed rainfall (2011–2020) from the closest meteorological station (Mt. Ampucao), a digital elevation model (DEM) derived from the nationwide 5 m IfSAR DEM acquired in 2013 (Grafil and Castro, 2014), field-derived sediment grain size distributions, and spatially variable bedrock erosion parameters for the mining area and the rest of the catchment (Figure 1 b, Table 1 and Table 2). Although higher-resolution LiDAR data exist for some floodplains, their spatial coverage is incomplete, so the IFSAR DEM was used to maintain a consistent vertical accuracy (1 m root-mean-square error). For computational efficiency, the 5 m IfSAR DEM was resampled to 20 m resolution using a bilinear interpolation algorithm. The field-derived grain size distribution was used uniformly throughout the model domain. It was derived from a bulk sediment sample collected within the wider basin (16.38° N, 120.69° E), in which 402 kg of sediment was processed through sequential sieving with progressively finer mesh sizes ranging from 180 mm to 0.064 mm, with the mass retained on each sieve was recorded. The detailed model inputs used in the simulation are listed in Table 1.

[1] caesar-lisflood download — SourceForge.net

Table 1: Model input datasets and sources

Input	Source	Resolution / Value
DEM	Interferometric Synthetic Aperture Radar (IfSAR; (Grafil and Castro, 2014))	20 m resampled from 5 m resolution IfSAR (2013) DEM using bilinear algorithm
Rainfall data	Local meteorological station (Mt. Ampucao) within Ambalanga catchment (Figure 1)	Hourly (2011–2020)
Sediment grain size distribution	Field-derived	9 classes (silt–gravel)
Erosion thresholds	Selected range of value based on previous research (Mitchell, 2014; Mitchell et al., 2013)	0.5 – 10 Pa
Erosion rates	Value replicating the historical event of 2018. In addition, the range of values set by reviewing previous research in the study area (Carating et al., 2014; Coxhead and Jayasuriya, 2004; Food and Agriculture Organization of the United Nations, 2001)	0.001 – 0.01 m/Pa/yr

3.3 Model Calibration: replicating the impact of 2018 debris flow event

The CAESAR-Lisflood model was initially set up and applied to replicate the impact of landslides and debris flows triggered by Typhoon Mangkhut on 15 September 2018 (National Disaster Risk Reduction and Management Council, 2018; Panici et al., 2024) in order to calibrate the model parameters. The calibration used observed hourly rainfall from 2014–2018 and the 2013 IfSAR-derived DEM, which represented the pre-event terrain. Before the 15 September 2018 event, the Mt. Ampucao station (Figure 1), located south of the Liang catchment, recorded an intense 24-hour rainfall of 528 mm, with a maximum hourly intensity of 67 mm. The calibration process focused on reproducing the geomorphic change caused by the 2018 debris-flow event, including TSF storage loss and sediment redistribution. The simulated post-event flood extents and TSF storage changes were compared with Google Earth satellite images (Figure 2), whilst erosion volumes and sediment transport were calibrated against the 2018 landslide inventory (National Disaster Risk Reduction and Management Council, 2018; Panici et al., 2024).

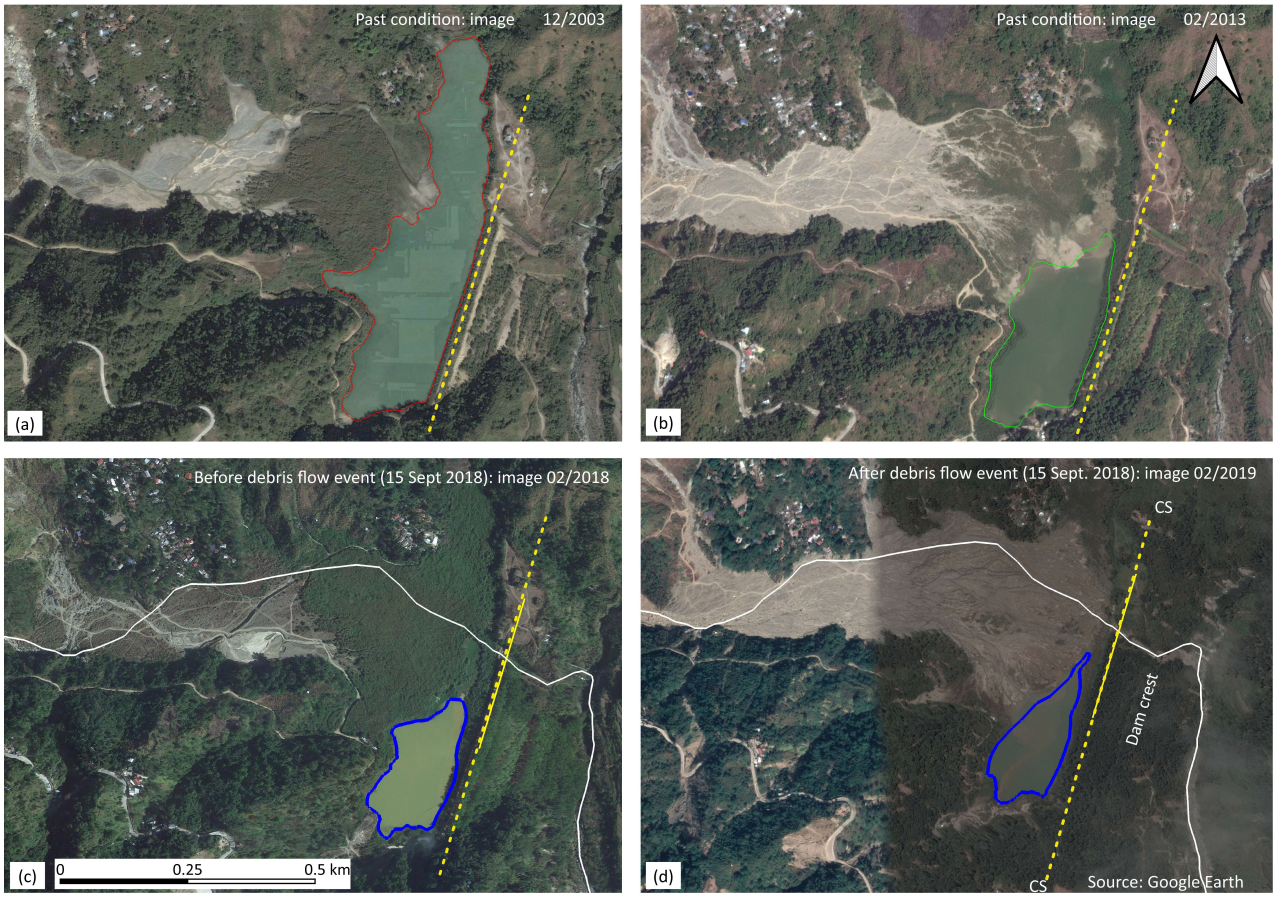

Figure 2: Satellite images of the tailings storage facility area (Figure 1) showing changes in the storage area over time. The storage boundaries were delineated by drawing polygons around the surface water extent: (a) 2003 storage area outlined by a solid red polygon (11.6 ha); (b) 2013 storage area outlined by a solid green polygon (5.75 ha), corresponding to the year the IfSAR DEM used in this study was acquired; (c) pre-event tailings storage facility area before the September 2018 event outlined by a solid blue polygon (3.51 ha); and (d) post-event tailings storage facility area after the September 2018 event outlined by a solid blue polygon (3.23 ha), with the dotted yellow line indicating the dam crest in all plots, and the solid white line marking the main channel in (c) and (d).

3.4 Scenario Design

Following model calibration, the observed rainfall record (2011–2020) was cyclically repeated for subsequent years to investigate TSF evolution over decadal to millennial timescales. To address our research objectives, 16 simulation scenarios were carried out (Table 2) in addition to the calibration run. To account for variability in TSF composition, we implemented a sensitivity analysis using a range of erodibility parameters for the bedrock erosion function in CL to simulate potential downcutting into the dam structure itself. The bedrock erosion function describes how bedrock is eroded by flowing water:

$$B = (\tau - \tau_c) * R, \tau > \tau_c \quad (1)$$

where, B is the bedrock erosion rate (m/yr); it is a function of the shear stress (τ) caused by flowing water (Pa) above a threshold (τ_c) needed for erosion to begin, and a factor (R) representing the erodibility of the bedrock (m/Pa/yr).

Given the uncertain composition of the Liang valley-fill TSF, we applied a range of plausible values for the erosion thresholds and rates, based on previous research in similar environments

(Carating et al., 2014; Coxhead and Jayasuriya, 2004; Food and Agriculture Organization of the United Nations, 2001; Mitchell, 2014; Mitchell et al., 2013). Specifically, bedrock erosion thresholds range from 0.5 to 10 (Pa) and erosion rates from 0.001 to 0.01 m/Pa/year, to cover a range of lithologies from relatively erodible bedrock to more resistant substrates. This framework enables evaluation of the relative influence of erosion thresholds versus erodibility on long-term sediment release and channel adjustment.

A total of 16 scenarios were tested to encompass the full range of erosion parameters. Each scenario combines the range of bedrock erosion thresholds (0.5–10 Pa) and bedrock erosion rates (0.001–0.01 m /Pa/year) for the tailings storage facility area. For clarity, hereafter, we refer to these parameters as 'dam erosion rates' and 'dam erosion thresholds', respectively. It is also important to note that different bedrock erosion rates and thresholds were defined for the rest of the catchment outside the tailings storage facility area (Table 2). In Table 2, Scenarios 1a–4c correspond to variable erosion parameters for both the TSF area and the rest of the catchment, whereas the Same Erosion (SE) scenarios apply to the same erosion parameters uniformly across the entire catchment. All scenarios were simulated over a 100-year period, except for Scenarios 1a and SE4, which ran for 1000 years to assess the long-term stability of the TSF.

Table 2: Scenario matrix: erosion thresholds and bedrock erosion rates

Scenarios	**Erosion Threshold, τ_c (Pa)**	**Erosion Rate, R (m/Pa/yr)**
Spatially varying erosion across the catchment		
Dam area		
1a–1c	1.0	0.01, 0.005, 0.0025
2a–2c	0.5	0.01, 0.005, 0.0025
3a–3c	2.0	0.01, 0.005, 0.0025
4a–4c	10.0	0.01, 0.005, 0.0025
Rest of the catchment excluding Dam area		
	10	0.001
Same Erosion (SE): uniform erosion parameters across the whole catchment		
SE1	1.0	0.001
SE2	0.5	0.001
SE3	2.0	0.001
SE4	10.0	0.001

3.5 Analysis of model outputs

After simulating all scenarios, we analysed the model outputs to evaluate the spatial patterns of erosion and deposition (using difference of the DEM output of the model from the initial DEM, DEM of difference (DoD); (James et al., 2012)), reduction in TSF storage (derived from water depth maps), dam wall erosion (by plotting longitudinal channel profiles over time), and sediment yields from the catchment. These analyses were used to assess the long-term impacts of the TSF. The sediment transport from the mining area and the rest of the catchment was traced in each simulation to quantify the ratio of sediment outflow from the open-pit mining area (red polygon in Figures 1 b and 1 e) relative to the rest of the catchment, to in turn evaluate sediment yields throughout the system.

4 Results

4.1 Model calibration

The calibrated model for the 15 September 2018 event effectively reproduced the observed flood extents and spatial patterns of erosion and sediment transport, aligning well with satellite-derived estimates. In more detail, the change in storage area determined from satellite images from before and after the September 2018 event indicated a loss of storage area of approximately 8%, from 3.51 to 3.23 ha (Figures 2 c and 2 d). Overlaying the simulated DoD and water depth maps from the 2018 event with the post-flood event satellite image (Figure 3) showed very similar patterns seen in the satellite image (Figure 2). The simulated water storage area upstream of the TSF after the 2018 event was found to be 3.0 ha (lime green polygon in Figure 3b), which is 7% lower than observed area (blue solid polygon in Figure 3d). Figure 4 shows the model output from 2014 to 2018, including the 15 September 2018 calibration event. The total simulated sediment outflow during this event was approximately 0.35 Mm^3 (height difference indicated by the grey dotted line in Figure 4) for the entire Liang catchment, of which 0.24 Mm^3 occurred within 500 m of the river channel. Sediment outflow traced from the mine site, from open pit mining to TSF, contributed up to 0.10 Mm^3 (height difference indicated by the red dotted line in Figure 4). This magnitude is comparable to the mapped cumulative landslide volumes (0.101–0.141 Mm^3) reported for the landslide cluster surrounding the TSF by Panici et al., 2024, providing confidence that the simulated sediment release from the mine area is of a similar order of magnitude to the independently estimated landslide-derived sediment inputs.

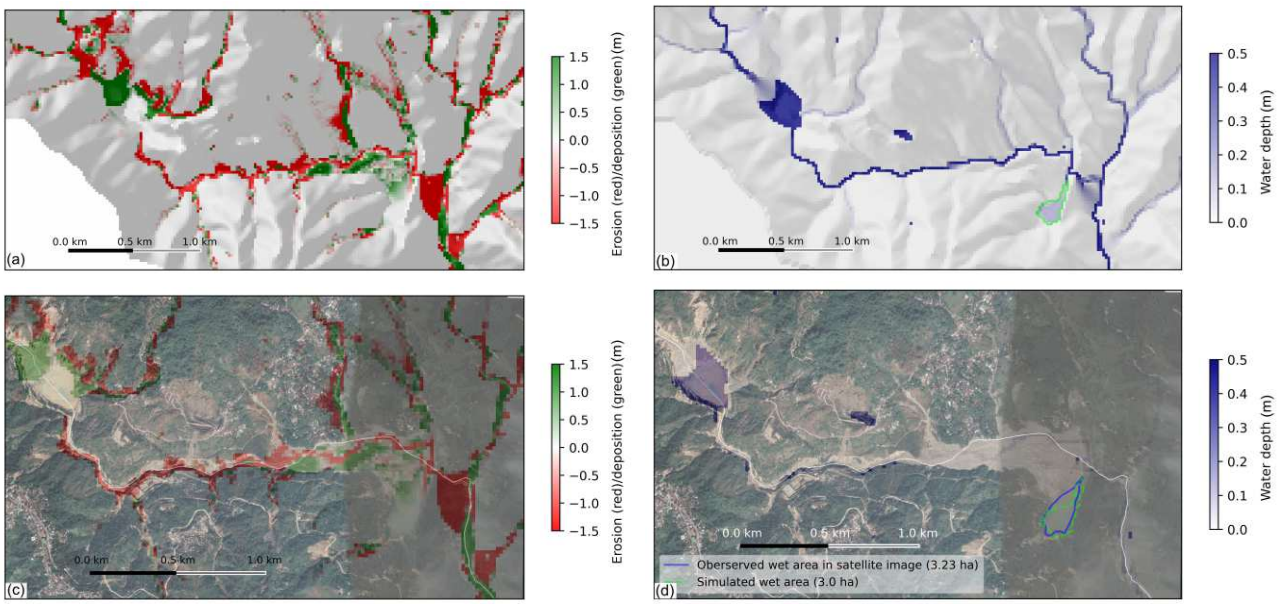

Figure 3: Simulated geomorphic and hydrodynamic responses in the Liang tailings storage facility area, overlaid on satellite imagery: (a) DEM of difference (DoD) map illustrating erosion (red) and deposition (green) before and after the September 2018 event; (b) Simulated water depth and inundation extent during the event, with the lime green polygon indicating the simulated water storage area; (c) and (d) Corresponding DoD and water depth maps overlaid on a satellite image acquired in February 2019, following the 2018 event. In (d), the green dotted line polygon represents simulated water storage, while the blue solid line polygon indicates observed water storage from the satellite image during the event.

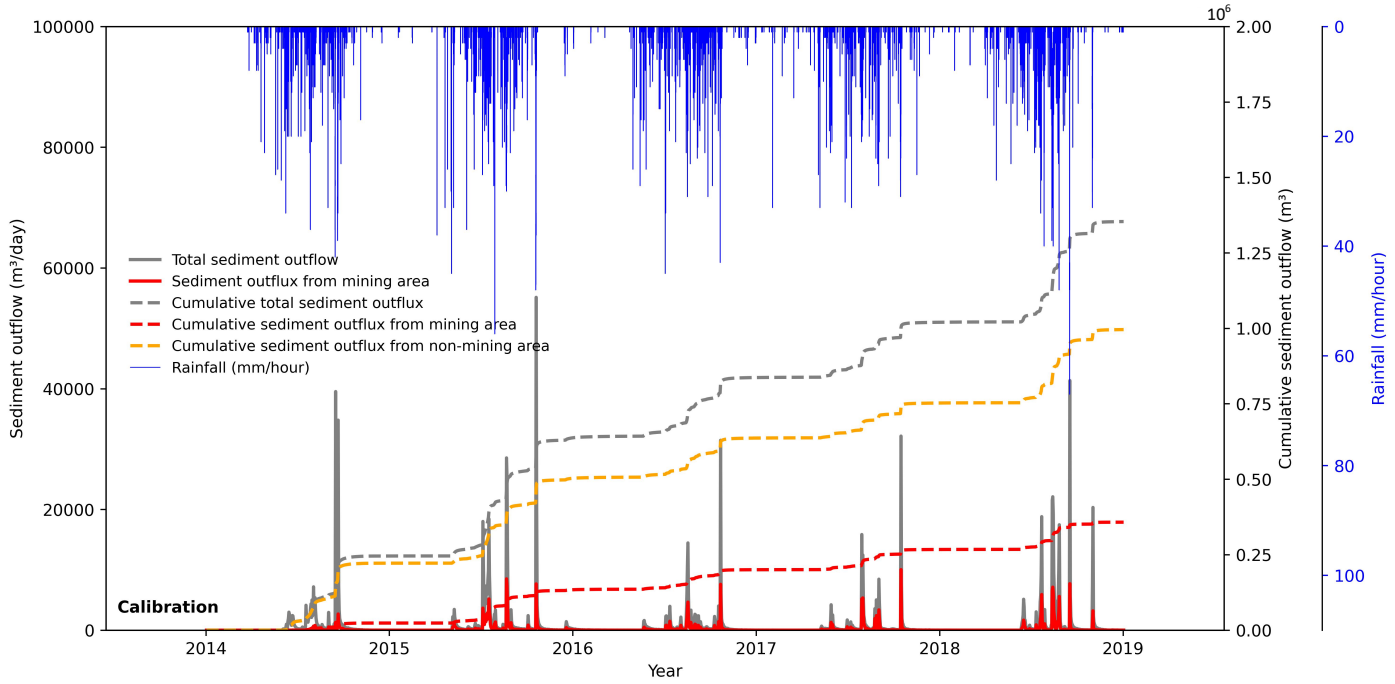

Figure 4: Simulated daily and cumulative sediment outflow from the entire catchment and mining area from 2014 to 2018 with hourly rainfall input.

4.2 Sediment transport and dam wall erosion under varying erosion Scenarios

Simulations carried out over centennial to millennial-year timescales revealed substantial variability in sediment yields and dam wall erosion depending on the erosion thresholds and dam erosion rates applied. Figure 5 compares sediment outflow under three scenarios (1a, 1b, and 1c), each with the same dam erosion threshold of 1.0 Pa but variable dam erosion rates of 0.01, 0.005, and 0.0025 m/Pa/yr, respectively (Table 2). The results showed a strong positive correlation between the dam erosion rate and sediment outflow, with higher erosion rates producing higher sediment outflow, particularly evident during the first three decades of the simulation (Figure 5). Despite these differences in short-term dynamics, total sediment outflow for both mining area and remaining catchment after 100 years was nearly identical between Scenarios 1a and 1b, both approximately 33% higher than Scenario 1c. Scenario 1a exhibited rapid initial outflow but transitioned to a slower rate beyond approximately 30 years, whilst Scenarios 1b and 1c maintain a steadier, more consistent increase throughout the simulation after the initial 10 years.

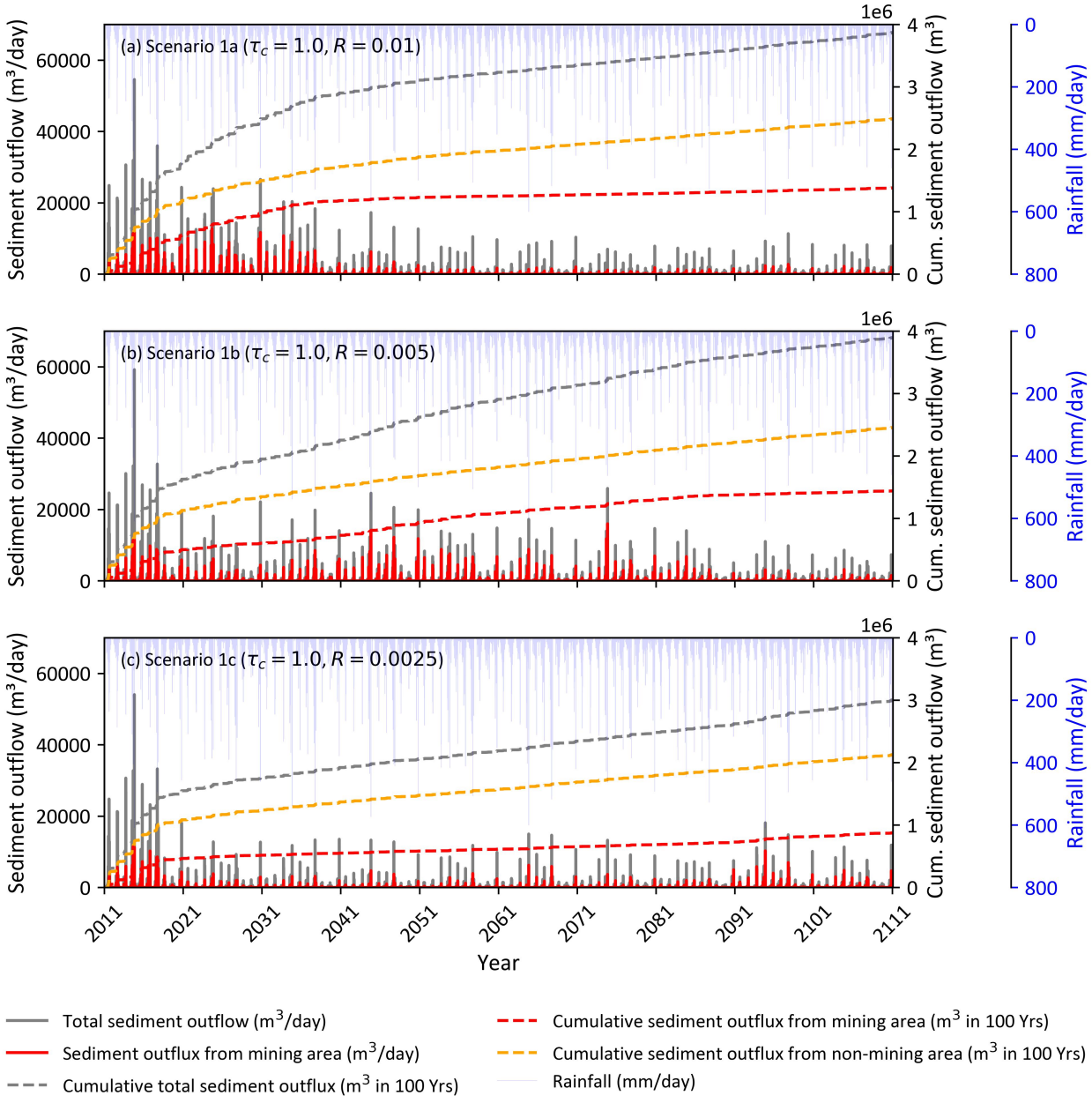

Figure 5: Daily and cumulative simulated sediment transport rate for 100 years using repeated observed rainfall from 2011 to 2020 for variable dam erosion rates with the same dam erosion threshold Scenarios of 1a, 1b, and 1c (see Table 2).

The longitudinal channel profiles for Scenarios 1a, 1b, and 1c (Figure 6a) exhibit clear evidence of progressive infilling in the upstream open-pit mining area (upstream in the long profiles in Figure 6a and red arrows on the left top corners of maps in Figure 1b). The long profiles show particularly within the first 50 years of simulation, and continuous downcutting and erosion of the Liang TSF. They also illustrate the gradual undercutting of the dam wall. The cross-sectional profiles across the dam crest (XS for Scenarios 1a, 1b, and 1c in Figure 6a) revealed substantial erosion of the dam wall, with maximum incision depths reaching up to 95 m in high-erosion Scenario 1a (longitudinal channel profile and cross-sectional profile at XS in Figure 6 a1 and a2). The erosion patterns initiated consistently in the spillway region (blue arrow in Figure 6b) and propagated downstream, contributing to a higher vertical incision in the dam structure. The incision rate was higher for the initial 50 years, but it slowed towards the end of the model run, possibly due to the defined bedrock level beneath the surface DEM.

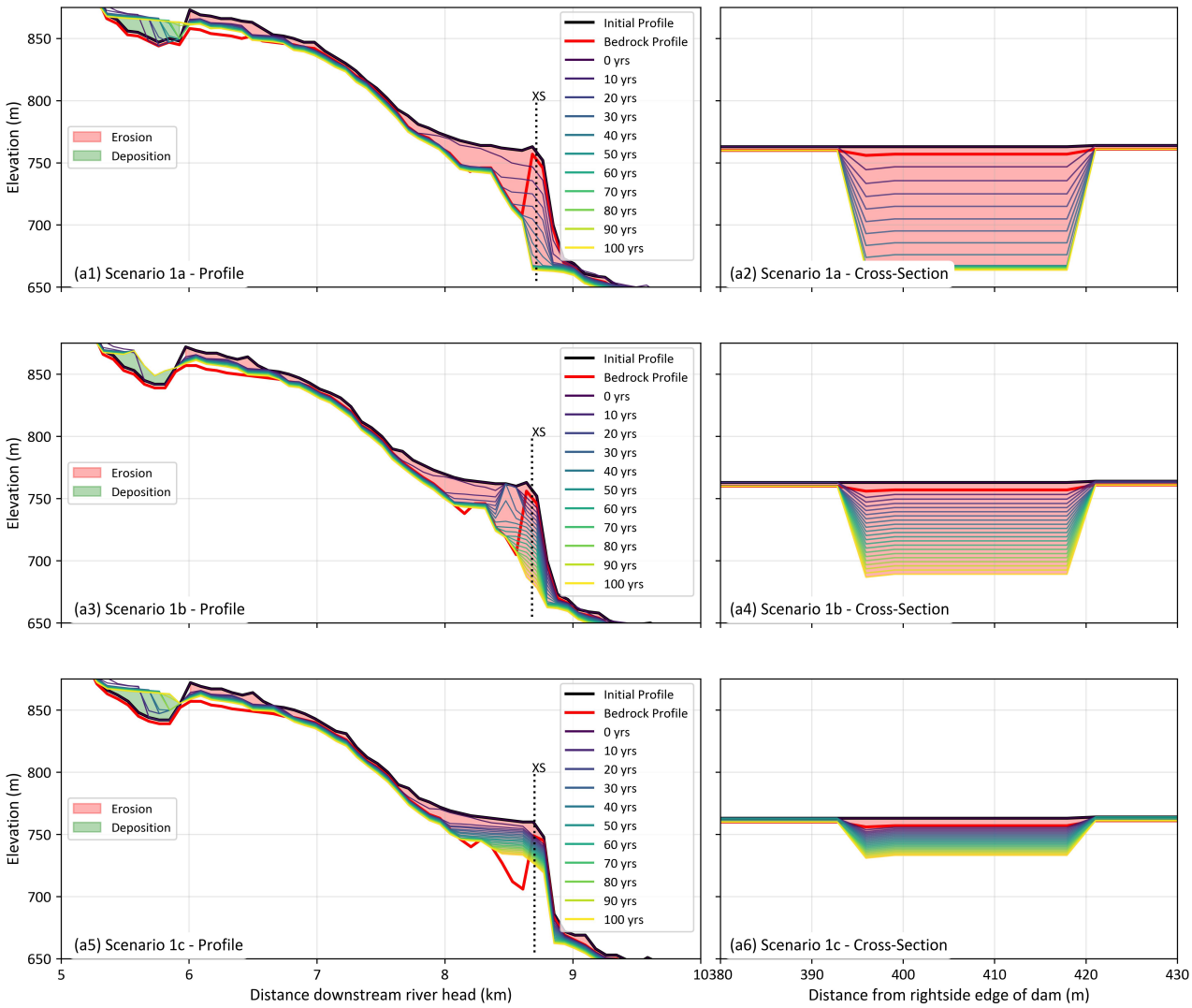

(a) Channel profile along channel thalweg and dam cross-section

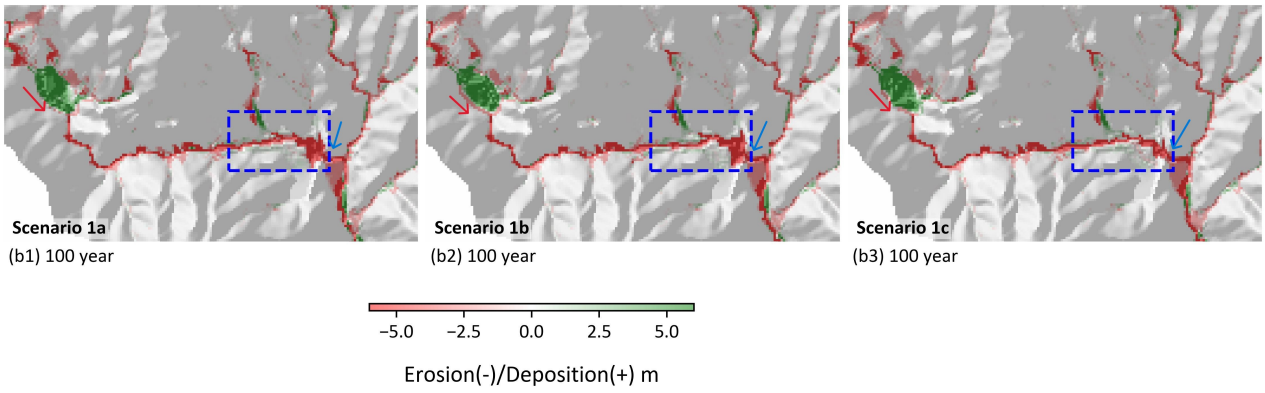

(b) Erosion and deposition maps

Figure 6: (a) Longitudinal channel profiles along the channel thalweg and corresponding dam crest cross-sections showing morphological changes over 100 years of simulation for (a1, a2) Scenario 1a, (a3, a4) Scenario 1b, and (a5, a6) Scenario 1c (see model scenarios in Table 2). The longitudinal profiles illustrate the progressive evolution of channel geometry, while the cross-sections highlight changes in channel width and bed elevation along the dam crest; (b) Spatial distributions of erosion and deposition derived from DEM of difference after 100 years of simulation for (b1) Scenario 1a, (b2) Scenario 1b, and (b3) Scenario 1c. Red and green regions represent erosion and deposition, respectively. The results indicate more pronounced channel widening under the higher dam erosion scenarios (1a and 1b) compared with the lower erosion scenario (1c), as highlighted by the blue dashed rectangles in b (b1-b3).

The DEM of Difference (DoD) maps (Figure 6b) show the significant decreases in TSF storage capacity lead to overtopping and redistribution of tailings downstream. There was slight lateral widening, primarily upstream of the TSF, which became more pronounced under higher erosion rate scenarios (see the blue dashed areas in the erosion/deposition maps in (Figure 6b) for scenarios 1a, 1b, and 1c). In scenarios with high erosion rates (e.g., 1a, 2a, 3a), the greater erodibility of dam material resulted in more rapid erosion, higher sediment mobility, and increased downstream redistribution. These results demonstrate that the erodibility of the dam material exerts a first-order control on the magnitude and timing of sediment release.

4.3 Morphology change of the tailings dam area

To evaluate the long-term integrity of the TSF, simulations were extended to 1,000 years for Scenario SE4 (Table 2), using uniform erosion parameters throughout the basin (bedrock erosion threshold: 10 Pa; rate: 0.001 m / Pa / year) and for Scenario 1a, which applied a lower erosion threshold (1.0 Pa) and higher erosion rate (0.01 m/Pa/year) to the dam material whilst retaining the SE4 values for the rest of the basin (Table 2). The higher erodibility of the dam material in Scenario 1a increased the cumulative sediment outflow from the catchment to 147 Mm^3over 1,000 years (Figure 7a). In Scenario SE4, where the dam material had a 10-fold lower erosion rate, the cumulative sediment outflow reached 120 Mm^3 over the same period (Figure 7b). Cumulative sediment outflow increased gradually throughout the 1,000-year simulation in both scenarios, indicating that long-term geomorphic adjustment continued even under conservative estimates of dam material erodibility.

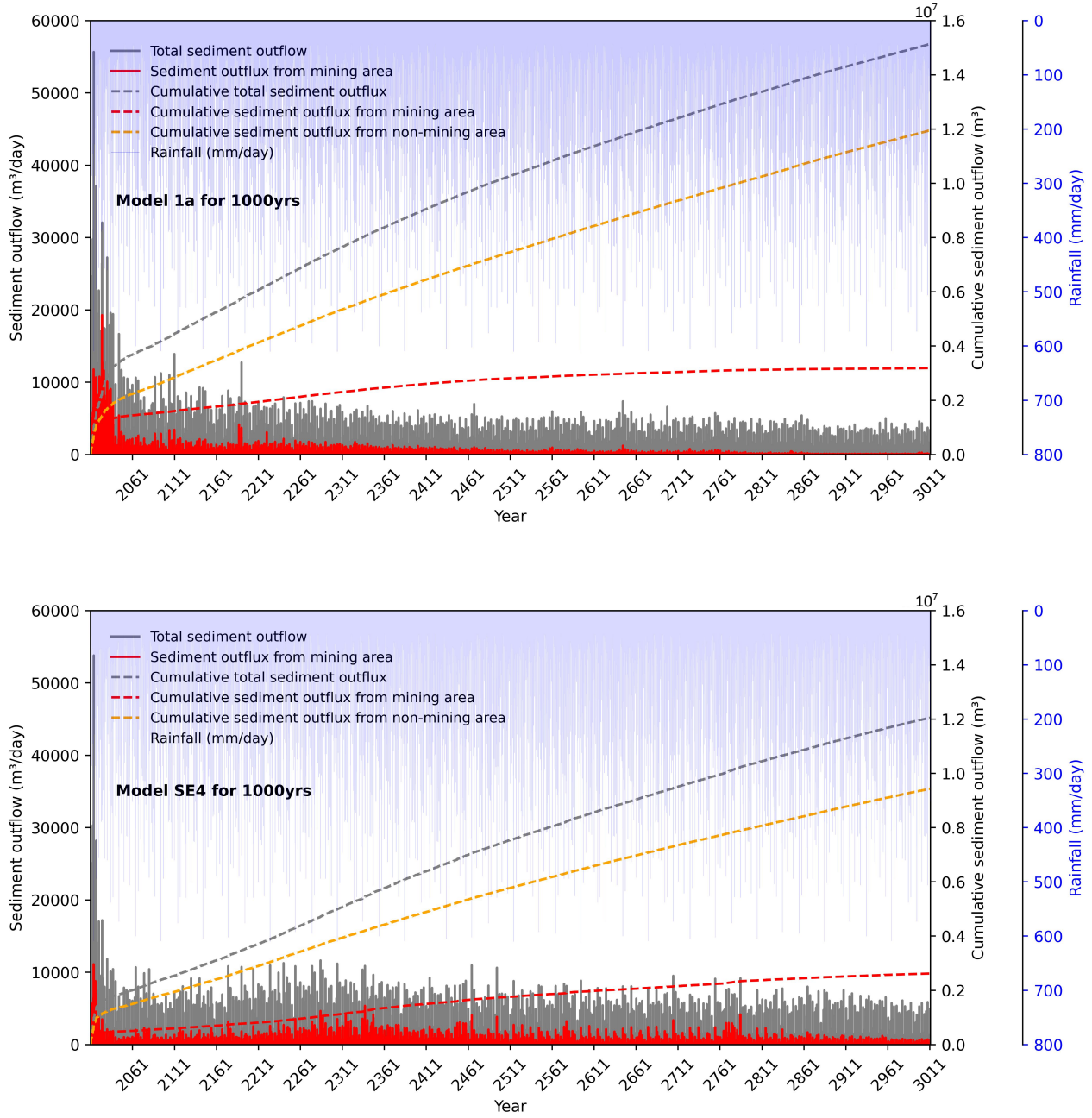

Figure 7: Sediment transport rates over a 1000-year simulation period (2011-3011): (a) Scenario 1a (τ_c = 1.0, R = 0.01), with spatially varying erosion thresholds and erosion rates between the dam area and the rest of the basin; and (b) Scenario SE4 (τ_c = 10.0, R = 0.001)), with uniform erosion threshold and erosion rate values throughout the basin.

The simulated temporal evolution of sediment erosion and deposition patterns (Figure 8) for the Scenario SE4 showed a phased morphological transformation of the TSF area. During the initial 10–50 years, accumulated sediment upstream (red arrow in Figure 8a) reduced the water storage capacity, gradually increasing the overtopping and incision at the location of the spillways, which also initiated the undercutting of the dam toe wall (red arrow in Figure 8b). After 100 years of simulation, moderate wall erosion was evident (red arrow in Figure 8c) with spatially concentrated incision along the spillway and adjacent slopes expanding laterally as well. At this stage, the upstream incision appeared predominantly vertical. After 1000 years of simulation, extensive erosion was observed at the dam crest (red arrow in Figure 8d), dam rear face (black arrow in Figure 8d), and upstream sections (blue and yellow arrow in Figure 8d),

indicating a transition from a structurally intact to a semi-breached landform. Throughout the simulation, notable deposition is also observed within the upstream open-pit mining site.

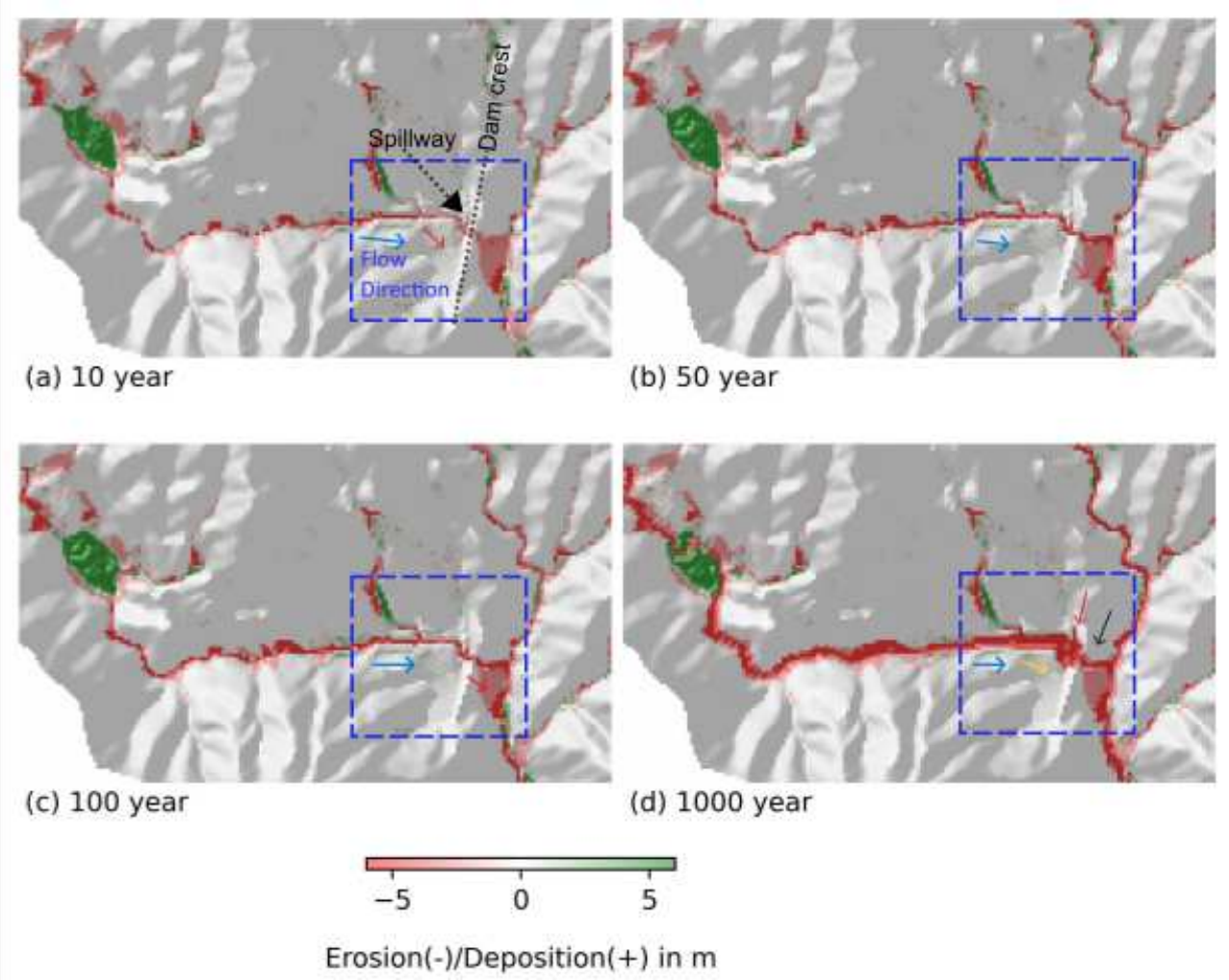

Figure 8: Simulated DEM of difference maps showing erosion (red as negative) and deposition (green as positive) after (a) 10; (b) 50; (c) 100; and (d) 1000 years of model simulation for the scenario SE4 and the blue arrows indicate the dominant sediment transport direction. The blue dotted rectangle highlights the TSF area with a spillway and dam crest marked by black dotted lines. The SE4 is the scenario representing a case where the same erosion parameters: both the bedrock erosion threshold (10 Pa) and the bedrock erosion rate (0.001 m/Pa/yr), are applied uniformly across the entire catchment, including the TSF area.

4.4 Sensitivity to erosion parameters

The sensitivity analysis of the bedrock erosion parameters showed that sediment transport from the catchment is more sensitive to the dam erosion rate than to the dam erosion threshold (Figure 9). Total sediment transported during the 100-year simulation ranged from approximately 2.51 to 4.38 Mm^3 (Figures 9c, 5, and Supplementary Figures S1-S4). The SE1-SE4 scenarios, with a constant dam erosion rate of 0.001 m/Pa/yr and erosion thresholds of 0.5, 1, 2, and 10 Pa, produced almost identical sediment transport (approximately 2.5 Mm^3), demonstrating that varying the erosion threshold had little influence on sediment transport. A similar trend was observed for variations in erosion thresholds at the other dam erosion rates of 0.0025, 0.005, and 0.01 m/Pa/yr, with only minor differences in total sediment transport. In contrast, increasing the dam erosion rate from 0.001 to 0.0025, 0.005, and 0.01 m/Pa/yr substantially increased sediment transport. For example, for a dam erosion threshold of 10 Pa (Scenarios

SE4, 4c, 4b, and 4a), total sediment transport increased from 2.54 to 3.11, 3.94, and 4.38 Mm^3 (Figure 9c), respectively. Sediment transported from the upstream mining area followed the same pattern as the total sediment transport from the catchment (Figures 9c and 9d), confirming that increased dam erodibility enhances sediment mobilisation throughout the system. Overall, these results indicate that long-term sediment transport is more sensitive to the dam erosion rate than to the dam erosion threshold.

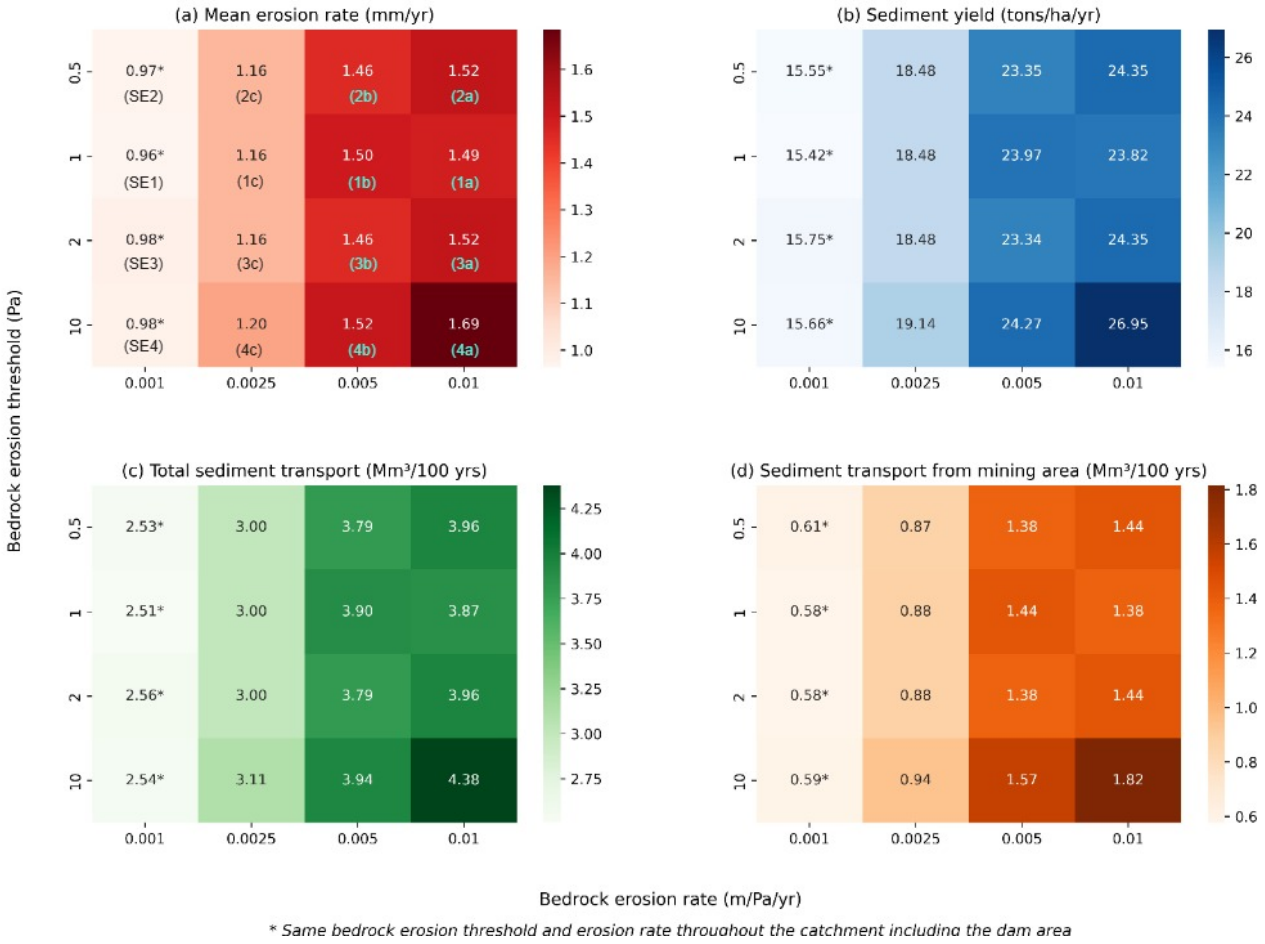

Figure 9: Heatmaps showing the impact of varying bedrock erosion thresholds and rates applied to the TSF on: (a) average erosion rate (mm/yr); (b) sediment yield (tons/ha/yr); (c) total sediment transport downstream over 100 years (Mm^3); and (d) sediment transport from upstream mining areas over 100 years (Mm^3). An asterisk (*) denotes scenarios where uniform erosion parameters were applied across the entire catchment, including the dam area.

Similarly, the average annual catchment erosion rate ranged from 0.98 to 1.69 mm/yr (Figure 9a), and sediment yield ranged from 15.66 to 26.95 tons/ha/yr (Figure 9b) as the dam erosion rate increased from 0.001 to 0.01 m/Pa/yr for a constant erosion threshold of 10 Pa. As observed for total sediment transport, both the average catchment erosion rate and sediment yield were more strongly influenced by the dam erosion rate than by the erosion threshold. For example, at a constant erosion threshold, doubling the dam erosion rate from 0.0025 to 0.005 m/Pa/yr increased catchment sediment yield by approximately 20–30%. In contrast, varying the erosion threshold between 0.5, 1, 2, and 10 Pa produced only minor changes in sediment yield (less than 10%) for a given dam erosion rate.

5 Discussion

5.1 What are the mechanisms and timescales associated with slow failure?

All the simulations showed that the slow TSF failure is driven by a positive feedback sequence: First, hydraulic freeboard reduces immediately upstream of the dam due to gradual sediment infilling. Second, this reduced freeboard leads to an increase in overtopping duration, for a given event, as well as an increase in overtopping frequency, as previously smaller flows behind the dam can now reach the crest. Third, overtopping itself leads to erosion of the crest, further reducing hydraulic freeboard. Fourth, overtopping also initiates spillway incision and erosion at the toe of the dam, which subsequently undermines the dam wall stability, causing further headward erosion of the dam wall, increasing erosion of the dam crest even more. In short, this combination of erosion and deposition generates a positive feedback loop: further reduced freeboard increases overtopping, which accelerates incision, further reducing freeboard (Figure 6). This progressive erosion mechanism is consistent with previous research on the long-term geomorphic evolution of tailings storage facilities, which highlighted overtopping and erosion as key controls on post-closure dam degradation (Bowker, Chambers, et al., 2016; Hancock and Coulthard, 2022; ICOLD, 2001; Sun et al., 2012).

The resistance of the dam material to erosion plays a key part in the timescales of failure. In the simulations, under high-erosion scenarios (e.g., (1-4) a), structural integrity is critically impacted within the first 30 years (Figures 6a1). Under moderate erosion rates (e.g., scenario (1-4) b and c, (Figures 6a3 and a5) , these slow failure pathways lead to visible morphological compromise within 50 years. In the model runs, dam wall erosion and upstream channel adjustments were front loaded, with more pronounced erosion during the first 10–50 years (Figure 6a1 and a3), again consistent with previous LEM studies showing concentrated early-phase transformation (Hancock and Coulthard, 2022; Slingerland et al., 2022). As the simulations progressed beyond 50 years, the resistance of the dam also played a key role controlling the geomorphic evolution of the area upstream and downstream of the dam with dam wall erosion and sediment transport continuing but at slower rates (Figure 6). In the higher dam erosion rate scenarios (1a: 0.01 and 1b: 0.005 m/Pa/yr; (Figure 6a1 and a3), the incision ultimately extends down to the base of the dam, i.e., down to the valley floor, whereas in the lower dam erosion rate scenario (1c: 0.0025), the incision was limited to about 30% of the dam height over the 100-year of simulation (Figure 6a5).

All the simulations demonstrated that TSFs and their surroundings underwent progressive transformation under natural hydrological and geomorphic processes, consistent with previous research by Slingerland et al., 2022 and Slingerland et al., 2018a. Given that TSFs remain part of the landscape long after mine closure, understanding their long-term geomorphic evolution beyond decadal to centennial timescales is critical for assessing their future stability and downstream impacts (McKenna and Van Zyl, 2020; Mittal and Morgenstern, 1975; Slingerland et al., 2022). Our findings suggest that, in geomorphically active river catchments such as those found across much of the Philippines, TSFs may become progressively compromised if left unmanaged after mine closure. The implications of these findings for post-closure management are discussed in Section 5.3.

Although overtopping is widely recognised as a major trigger of rapid tailings storage facility failure (Bowker, Chambers, et al., 2016; ICOLD, 2001; Sun et al., 2012), our simulations demonstrate how the combination of local geomorphic processes (leading to dam infilling) may cause repeated overtopping and progressive erosion controlled by the erodibility of the dam. Our simulated sequence of infilling and overtopping mirrors natural valley-fill incision processes and suggests that functional failure (e.g., overflow or progressive breach) can occur within decades to centuries under present-day rainfall conditions (Hancock and Coulthard, 2022). Our findings

clearly agree with previous studies that highlighted that TSFs should be regarded as evolving landforms rather than static infrastructure (Hancock and Coulthard, 2022; McKenna and Van Zyl, 2020).

5.2 How much sediment can be released downstream and what are the implications?

In high-erosion scenarios (e.g., 1a, 2a, 3a, and 4a), the sediment yields of the catchment increased substantially as the rate of dam wall erosion also increased. Therefore, the construction of the dam itself exerts first-order control over the amount of sediment released. The longitudinal profile plots (Figure 6a) showed the headward incision upstream of the TSF, working through sediments deposited behind it. The re-working of this previously stored sediment represents two potential hazards. First, in an area that was heavily mined, the sediment and stored tailings may have high concentrations of potentially toxic metal(loid)s and other elements that could present a hazard to downstream habitats and communities. Second, deposition of sediment and tailings downstream can negatively impact infrastructure, agriculture, ecosystems and local communities (Hudson-Edwards et al., 2024). As shown in Figures 6 and 9 tailings mobilisation is not just a short-term hazard, but a long-term risk that can reshape downstream river systems and ecosystems.

The volume and duration of downstream sediment release depend strongly on the dam erosion rate and dam wall erodibility. Our results show that even low-erodibility dams (e.g., SE4) can release more than 3 $Mm^3$of sediment within the first 100 years and up to 120 Mm^3 over 1000 years. In contrast, high-erodibility scenarios such as Scenario 1a release approximately 4 Mm^3 in just 100 years and up to 147 Mm^3 over a 1000-year period (Figure 7). Rapid wall failure produces an early pulse of sediment within the first 30 years, whereas slower erosion yields similar total sediment outflows but over more extended timescales (100+ years). Importantly, while the total sediment output is comparable, hazard types differ significantly. In both fast and slow failure scenarios, total sediment exports are similar, but hazard types differ: rapid failure generates large early pulses, while gradual erosion sustains downstream sediment delivery and contamination for centuries, a risk underappreciated in many standard TSF assessments (Hudson-Edwards et al., 2024);however, contaminant transport was not modelled in this study.
.

5.3 Implications for TSF management, future modelling approaches and model limitations?

This study highlights that the slow failure process of TSF can cause significant impacts. TSF planning should thus incorporate geomorphic evolution and slow failure pathways throughout the facility life cycle, from site selection and design to operation, closure, and post-closure management. Early planning should consider how TSF construction, filling, and long-term landscape evolution may alter the catchment, so that these changes can be anticipated and mitigated through design and management. The existing abandoned TSFs require long-term post-closure monitoring and management, consistent with the recommendations of the Global Industry Standard on Tailings Management (GISTM)* (International Council on Mining and Metals (ICMM), United Nations Environment Programme (UNEP), and Principles for Responsible Investment (PRI), 2020). In dynamic landscape settings such as the Philippines, where intense monsoonal rainfall and frequent typhoons accelerate geomorphic processes, this perspective is particularly urgent. Our findings closely align with (Reyes et al., 2023), who highlighted the vulnerability of legacy TSFs in the Philippines due to intense rainfall, limited post-closure management, and dynamic geomorphological settings. It is therefore vital to consider that future increases in storm magnitude and frequency associated with climate change in

the Philippines (Tolentino et al., 2025) are likely to doubly impact by increasing sediment delivery to fill a TSF as well as increase flood flows that promote overtopping (Labonté-Raymond et al., 2020). The processes and mechanisms we have simulated in this study are based in the tropical Philippines but are in our view very applicable to many mined landscapes and TSFs across the world.

For this purpose, the CAESAR-Lisflood model proved valuable for exploring long-term erosion patterns, infilling, and wall degradation in a real-world setting. However, the model carries important limitations. Vegetation cover was treated as spatially uniform and temporally constant, omitting the effects of seasonal drought, typhoon-driven disturbance, and progressive colonisation by woody species, all of which can substantially alter surface erodibility and water loss through transpiration (Hancock and Coulthard, 2022). A single spatially uniform grain size distribution was applied across the model domain, whereas the Liang TSF in reality comprises heterogeneous materials with contrasting erodibilities in the impoundment and dam wall. The model also does not simulate geotechnical instability or tailings consolidation, which may interact with surface erosion processes to influence dam wall integrity (McKenna and Van Zyl, 2020). Critically, the absence of chemical transport processes means that the downstream dispersal and environmental fate of potentially toxic metal(loid)s contained within the tailings were not assessed, a key priority for future interdisciplinary research.

6 Conclusions

This study presents the first application of the CAESAR-Lisflood landscape evolution model to simulate the long-term evolution and failure (decadal to millennial timescale) of a real-world abandoned valley-fill TSF (Liang/Antamok tailings storage facility) in a geomorphically dynamic river system. By modelling river geomorphic change over decadal-to-millennial time scales under observed rainfall conditions, we demonstrate that inactive TSFs can function as evolving anthropogenic landforms that continue to influence sediment mobility, channel adjustment, and downstream morphology long after mine closure. Recognising this continued geomorphic activity requires that regulatory and stewardship frameworks extend well beyond the operational lifespan of a facility. Even for low to moderate dam erosion rates, progressive reservoir infilling, spillway incision, dam toe cutting, and dam wall retreat further reduce storage capacity and structural integrity over time. Although the most rapid adjustments occur within the first decades, geomorphic transformation persists over centuries, progressively reshaping both the dam structure and downstream landscapes requiring that post-closure governance frameworks reflect their continued geomorphic activity.

A key mechanism driving gradual TSF failure is the reduction of hydraulic freeboard through progressive sediment infilling, which increases overtopping frequency and initiates a self-reinforcing erosion cascade. This gradual pathway represents a persistent, cumulative hazard with significant implications for downstream sedimentation and, in contaminated settings, for the long-term dispersal of potentially toxic metal(loid)s. Gradual failure must therefore be recognised as a significant but commonly underappreciated long-term hazard pathway in TSF risk assessment. The sensitivity analysis indicated that the long-term evolution of tailings storage facilities is primarily controlled by erodibility of dam material, while critical erosion thresholds exert a secondary influence. Small variations in erosion rates may produce nonlinear amplification of long-term sediment flux and channel response, underscoring the importance of material properties for post-closure management planning. Future research should integrate climate-change scenarios, contaminant transport modelling, and geotechnical frameworks to provide robust forecasts of TSF evolution, downstream impacts, and long-term risk, building on the process-based approach demonstrated here.

7 Data availability

This research used open-source software with minor modifications. The model results, maps, and associated data are available from the authors on reasonable request.

Paper Highlights

- Simulates the long-term geomorphic evolution of an inactive tailings storage facility and highlights the gradual failure mechanism over centuries to millennia.
- The CAESAR–Lisflood model is applied and calibrated against a past debris flow event.
- Sediment infilling reduces dams' storage capacity and can promote overtopping.
- Dam-material erodibility influences sediment transport, spillway incision and channel evolution.
- Inactive TSFs can remain geomorphically active long after mine closure.

References

Abancó, C., G. L. Bennett, A. J. Matthews, M. A. M. Matera, and F. J. Tan (2021). "The role of geomorphology, rainfall and soil moisture in the occurrence of landslides triggered by 2018 Typhoon Mangkhut in the Philippines". In: *Natural Hazards and Earth System Sciences* 21.5, pp. 1531–1550. URL: https://nhess.copernicus.org/articles/21/1531/2021/.

Aggangan, N. S., J. A. Anarna, and N. M. Cadiz (2019). "Tree legume–microbial symbiosis and other soil amendments as rehabilitation strategies in mine tailings in the Philippines". In: *Philipp J Sci* 148.3, pp. 481–491. URL: https://www.researchgate.net/publication/335867683_Tree_Legume_-Microbial_Symbiosis_and_Other_Soil_Amendments_as_Rehabilitation_Strategies_in_Mine_Tailings_in_the_Philippines.

Armstrong, M., N. Langrené, R. Petter, W. Chen, and C. Petter (2019). "Accounting for tailings dam failures in the valuation of mining projects". In: *Resources Policy* 63, p. 101461. URL: https://doi.org/10.1016/j.resourpol.2019.101461.

Azam, S. and Q. Li (2010). "Tailings dam failures: A review of the last one hundred years". In: *Geotechnical News* 28.4, pp. 50–54.

Bates, P. D., M. S. Horritt, and T. J. Fewtrell (2010). "A simple inertial formulation of the shallow water equations for efficient two-dimensional flood inundation modelling". In: *Journal of hydrology* 387.1-2, pp. 33–45. URL: https://www.sciencedirect.com/science/article/pii/S0022169410001538.

Benguet Corporation (2026). *Our Company*. Accessed: 28 July 2026. URL: https://benguetcorp.com/about-us/our-company/.

Boothroyd, R. J., R. D. Williams, T. B. Hoey, G. J. Brierley, P. L. Tolentino, E. L. Guardian, et al. (2025). "Big data show idiosyncratic patterns and rates of geomorphic river mobility". In: *Nature communications* 16.1, p. 3263. URL: https://doi.org/10.1038/s41467-025-58427-9.

Boothroyd, R. J., R. D. Williams, T. B. Hoey, C. MacDonell, P. L. M. Tolentino, L. Quick, et al. (Mar. 2023). "National-scale geodatabase of catchment characteristics in the Philippines for river management applications". In: *PLOS ONE* 18.3, pp. 1–25. URL: https://doi.org/10.1371/journal.pone.0281933.

Bowker, L. N., D. M. Chambers, et al. (2016). "Root causes of tailings dam overtopping: the economics of risk & consequence". In: URL: http://dx.doi.org/10.25675/10217/179793.

Carating, R. B., R. G. Galanta, and C. D. Bacatio (2014). *The soils of the Philippines*. Springer. URL: https://link.springer.com/content/pdf/10.1007/978-94-017-8682-9.pdf.

Chaloping-March, M. (2017). *Social Terrains of Mine Closure in the Philippines*. 1st. Routledge. DOI: 10.4324/9781315177182.

Chandler, R. J. and G. Tosatti (Apr. 1995). "The Stava Tailings Dams Failure, Italy, July 1985." In: *Proceedings of the Institution of Civil Engineers - Geotechnical Engineering* 113.2, pp. 67–79. DOI: 10.1680/igeng.1995.27586.

Corpus, T., C. David, S. Murao, and V. Maglambayan (2011). "Smallscale gold Mining in the Ambalanga Catchment, Philippines: its control on mercury methylation in stream sediments". In: *International Journal of Environmental Sciences* 2.2, pp. 1048–1059.

Coulthard, T. J., J. C. Neal, P. D. Bates, J. Ramirez, G. A. de Almeida, and G. R. Hancock (2013). "Integrating the LISFLOOD-FP 2D hydrodynamic model with the CAESAR model: implications for modelling landscape evolution". In: *Earth Surface Processes and Landforms* 38.15, pp. 1897–1906.

Coxhead, I. and S. Jayasuriya (2004). "Development strategy and trade liberalization: implications for poverty and environment in the Philippines". In: *Environment and Development Economics* 9.5, pp. 613–644. URL: https://doi.org/10.1017/S1355770X04001445.

Cultural Survival (July 2023). *Indigenous Peoples Continue 100-year Fight Against Large-Scale Gold Mining in the Philippines*. https://www.culturalsurvival.org/news/

indigenous-peoples-continue-100-year-fight-against-large-scale-gold-mining-philippines. Accessed: 2025-09-05.

Dethier, E. N., C. E. Renshaw, and F. J. Magilligan (2022). "Rapid changes to global river suspended sediment flux by humans". In: *Science* 376.6600, pp. 1447–1452. URL: https://www.science.org/doi/abs/10.1126/science.abn7980.

Domingo, E. G. (1993). "The Philippine mining industry: status and trends in mineral resources development". In: *Journal of Southeast Asian Earth Sciences* 8.1. Seventh Regional Congress on Geology, Mineral and Energy Resources of Southeast Asia, pp. 25–36. URL: https://www.sciencedirect.com/science/article/pii/0743954793900049.

Domingo, J. P. T., G. R. Jenkin, L. Quick, R. D. Williams, K. A. Hudson-Edwards, C. Tortajada, et al. (2024). "Sustainable mining in tropical, biodiverse landscapes: Environmental challenges and opportunities in the archipelagic Philippines". In: *Journal of Cleaner Production*, p. 143114. URL: https://doi.org/10.1016/j.jclepro.2024.143114.

Dong, L., S. Deng, and F. Wang (2020). "Some developments and new insights for environmental sustainability and disaster control of tailings dam". In: *Journal of Cleaner Production* 269, p. 122270. URL: https://doi.org/10.1016/j.jclepro.2020.122270.

DOST-PAGASA (2023). *Climatological data*. https://www.pagasa.dost.gov.ph/climate/climate-data. Department of Science and Technology, Philippine Atmospheric, Geophysical and Astronomical Services Authority. Accessed: 2025-05-21.

Eriksson, N. and M. Adamek (2016). "The tailings pond failure at the Aznalcóllar mine, Spain". In: *Proceedings of the BC Mine Reclamation Symposium*. URL: https://bc-mlard.ca/files/presentations/2016-19-ERIKSSON-ADAMEK-tailings-pond-failure-aznalcollar.pdf.

Food and Agriculture Organization of the United Nations (2001). *Chapter 3: Food Security*. Accessed: 2025-06-05. FAO. URL: https://www.fao.org/4/ab604e/ab604e03.htm.

Foundation, S. 1. (2003). *The Aznacóllar tailings dam failure, 1998*. URL: https://www.stava1985.it/aznacollar-mine-reservoir-collapse-spain/?lang=en.

Grafil, L. and O. Castro (2014). "Acquisition of IfSAR for the production of nationwide DEM and ORI for the Philippines under the unified mapping project". In: *Infomapper* 21.12-13, pp. 40–43.

Guardian (Sept. 2018). "Mangkhut leaves death, destruction and chaos from Philippines to China". In: *The Guardian*. Accessed: 2025-05-23. URL: https://www.theguardian.com/world/2018/sep/17/mangkhut-leaves-death-destruction-and-chaos-from-philippines-to-china.

Hancock, G. R. and T. J. Coulthard (2022). "Tailings dams: Assessing the long-term erosional stability of valley fill designs". In: *Science of The Total Environment* 849. DOI: 10.1016/j.scitotenv.2022.157692.

Hancock, G. (2021). "A method for assessing the long-term integrity of tailings dams". In: *Science of the Total Environment* 779, p. 146083. URL: https://doi.org/10.1016/j.scitotenv.2021.146083.

Hudson-Edwards, K. A., D. Kemp, L. A. Torres-Cruz, M. G. Macklin, P. A. Brewer, J. R. Owen, et al. (2024). "Tailings storage facilities, failures and disaster risk". In: *Nature Reviews Earth & Environment* 5.9, pp. 612–630. URL: https://doi.org/10.1038/s43017-024-00576-4.

Hudson-Edwards, K. A., H. E. Jamieson, and B. G. Lottermoser (2011). "Mine wastes: past, present, future". In: *Elements* 7.6, pp. 375–380. URL: https://doi.org/10.2113/gselements.7.6.375.

ICOLD, U. (2001). "Tailings dams–risk of dangerous occurrences, lessons learnt from practical experiences (bulletin 121)". In: *Commission Internationale des Grands Barrages, Paris* 155.

International Council on Mining and Metals (ICMM), United Nations Environment Programme (UNEP), and Principles for Responsible Investment (PRI) (2020). *Global Industry Standard*

on Tailings Management. Accessed: 2025-09-05. URL: https://globaltailingsreview.org/global-industry-standard/.

James, L. A., M. E. Hodgson, S. Ghoshal, and M. M. Latiolais (2012). "Geomorphic change detection using historic maps and DEM differencing: The temporal dimension of geospatial analysis". In: *Geomorphology* 137.1, pp. 181–198. URL: https://doi.org/10.1016/j.geomorph.2010.10.039.

Jessie, S., G. C. Reven, T. Alexandria, R. Rasty, M. Norman, and R. C. Darwin (2020). "Comprehensive assessment on the environmental conditions of abandoned and inactive mines in the Philippines". In: *ASEAN Journal on Science and Technology for Development* 37.2, p. 8. URL: https://ajstd.ubd.edu.bn/journal/vol37/iss2/8/.

Kossoff, D., W. Dubbin, M. Alfredsson, S. Edwards, M. Macklin, and K. Hudson-Edwards (2014). "Mine tailings dams: Characteristics, failure, environmental impacts, and remediation". In: *Applied Geochemistry* 51, pp. 229–245. URL: https://www.sciencedirect.com/science/article/pii/S0883292714002212.

Labonté-Raymond, P.-L., T. Pabst, B. Bussière, and É. Bresson (2020). "Impact of climate change on extreme rainfall events and surface water management at mine waste storage facilities". In: *Journal of Hydrology* 590, p. 125383. URL: https://doi.org/10.1016/j.jhydrol.2020.125383.

Liu, D., H. Yang, C. Lu, W. Wang, Q. Gu, and S. Ruan (2026). "An intelligent approach to prediction of tailings dam displacement safety using dynamic preventive control modeling". In: *Green and Smart Mining Engineering*. URL: https://doi.org/10.1016/j.gsme.2025.10.008.

Lowry, J., T. Coulthard, and G. Hancock (2013). "Assessing the long-term geomorphic stability of a rehabilitated landform using the CAESAR-Lisflood landscape evolution model". In: *Mine Closure 2013: Proceedings of the Eighth International Seminar on Mine Closure*. Ed. by M. Tibbett, A. Fourie, and C. Digby. Cornwall: Australian Centre for Geomechanics, pp. 611–624. DOI: 10.36487/ACG_rep/1352_51_Lowry.

Macasieb, R. Q., C. R. Orozco, and A. C. Resurreccion (2021). "Heavy metal contamination assessment and source apportionment analysis using multivariate methods in surface sediments of mining-impacted rivers in Benguet". In: *International Journal of Environmental Studies* 78.2, pp. 283–300. URL: https://doi.org/10.1080/00207233.2020.1802953.

Macklin, M., P. Brewer, K. Hudson-Edwards, G. Bird, T. Coulthard, I. Dennis, et al. (2006). "A geomorphological approach to the management of rivers contaminated by metal mining". In: *Geomorphology* 79.3, pp. 423–447. URL: https://www.sciencedirect.com/science/article/pii/S0169555X06002613.

Macklin, M. G., C. Thomas, A. Mudbhatkal, P. Brewer, K. Hudson-Edwards, J. Lewin, et al. (2023). "Impacts of metal mining on river systems: a global assessment". In: *Science* 381.6664, pp. 1345–1350. URL: https://doi.org/10.1126/science.adg6704.

Mahdi, A., A. Shakibaeinia, and Y. B. Dibike (2020). "Numerical modelling of oil-sands tailings dam breach runout and overland flow". In: *Science of the Total Environment* 703, p. 134568. URL: https://doi.org/10.1016/j.scitotenv.2019.134568.

McKenna, G. and D. Van Zyl (2020). "Chapter VIII: Closure and reclamation". In: *Towards Zero Harm: A Compendium of Papers Prepared for the Global Tailings Review*. Ed. by B. Oberle, D. Brereton, and A. Mihaylova. Accessed May 2025. St Gallen, Switzerland: Global Tailings Review, pp. 109–125. URL: https://globaltailingsreview.org/.

Mitchell, N. C. (Oct. 2014). "Bedrock erosion by sedimentary flows in submarine canyons". In: *Geosphere* 10.5, pp. 892–904. eprint: https://pubs.geoscienceworld.org/gsa/geosphere/article-pdf/10/5/892/3335737/892.pdf. URL: https://doi.org/10.1130/GES01008.1.

Mitchell, N. C., J. M. Huthnance, T. Schmitt, and B. Todd (2013). "Threshold of erosion of submarine bedrock landscapes by tidal currents". In: *Earth Surface Processes and Landforms* 38.6, pp. 627–639. DOI: https://doi.org/10.1002/esp.3347.

Mittal, H. K. and N. R. Morgenstern (1975). "Parameters for the design of tailings dams". In: *Canadian Geotechnical Journal* 12.2, pp. 235–261. URL: https://doi.org/10.1139/t75-028.

Mudd, G. and D. V. Boger (2013). "The ever growing case for paste and thickened tailings—towards more sustainable mine waste management". In: *J. Aust. Inst. Min. Metall* 2, pp. 56–59.

National Disaster Risk Reduction and Management Council (2018). *Preparedness Measures and Effects for Typhoon "OMPONG" (I.N. "MANGKHUT").* Tech. rep. SitRep No. 48. Accessed on 09/05/2025. Quezon City, Philippines: National Disaster Risk Reduction and Management Council. URL: http://ndrrmc.gov.ph/attachments/article/3437/SitRep_No_48_re_Preparedness_Measures_and_Effects_for_Typhoon_OMPONG_IN_MANGKHUT_as_of_6PM_28_Sept_2018_to_6AM_29_Sept_2018.pdf.

Panici, D., G. L. Bennett, R. J. Boothroyd, C. Abancó, R. D. Williams, F. Tan, et al. (2024). "Observations and computational multi-phase modelling in tropical river settings show complex channel changes downstream from rainfall-triggered landslides". In: *Earth Surface Processes and Landforms* 49.8, pp. 2498–2516. URL: https://onlinelibrary.wiley.com/doi/abs/10.1002/esp.5841.

Philippine Securities and Exchange Commission (PSEC) (Nov. 2016). *Press Release on the Reported Mine Tailings Leak in Antamok Mine of Benguet Corporation (SEC Form 17-C).* Accessed: 2025-07-31. URL: http://edge.pse.com.ph/openDiscViewer.do?edge_no=518ec103e89b0ab972785c150f4cd6d2#sthash.1ArMpy72.dpbs.

Reyes, G., R. Luna, P. Selda, J. Tanap, R. Gonzales, and J. Pallarca (2023). "Tailings Storage Facilities in the Philippines: Environmental, Geotechnical and Seismic Design Considerations". In: *In 9th International Congress on Environmental Geotechnics (ICEG2023).* URL: https://doi.org/10.53243/ICEG2023-358.

Saynor, M. J., J. B. Lowry, and J. M. Boyden (2019). "Assessment of rip lines using CAESAR-Lisflood on a trial landform at the Ranger Uranium Mine". In: *Land Degradation & Development* 30.5, pp. 504–514. URL: https://onlinelibrary.wiley.com/doi/abs/10.1002/ldr.3242.

Slingerland, N., N. Beier, and G. Wilson (2018a). "Landscape evolution modelling of large sand tailings dams". In: *Proceedings of the 2018 International Mine Closure Conference*, pp. 341–348.

Slingerland, N., N. Beier, and G. Wilson (2019). "Stress testing geomorphic and traditional tailings dam designs for closure using a landscape evolution model". In: *Mine Closure 2019: Proceedings of the 13th International Conference on Mine Closure.* Australian Centre for Geomechanics, pp. 1533–1544. URL: https://doi.org/10.36487/ACG_rep/1915_120_Slingerland.

Slingerland, N., F. Zhang, and N. Beier (2022). "Sustainable design of tailings dams using geotechnical and geomorphic analysis". In: *CIM Journal* 13.1, pp. 1–15. URL: https://doi.org/10.1080/19236026.2022.2027077.

Slingerland, N., A. Isidoro, S. Fernandez, and N. A. Beier (2018b). "Geomorphic analysis for tailings dam design in consideration of a 1000-year closure design life". In: *Proceedings of the 2nd International Congress on Planning for Closure of Mining Operations*, pp. 1–9.

Sun, E., X. Zhang, Z. Li, and Y. Wang (2012). "Tailings Dam Flood Overtopping Failure Evolution Pattern". In: *Procedia Engineering* 28. 2012 International Conference on Modern Hydraulic Engineering, pp. 356–362. URL: https://doi.org/10.1016/j.proeng.2012.01.733.

Thomson, H. and L. Chandler (2019). "Tailings storage facility landform evolution modelling". In: *Mine closure 2019: Proceedings of the 13th international conference on mine closure*. Australian Centre for Geomechanics, pp. 385–396. URL: https://doi.org/10.36487/ACG_rep/1915_31_Thomson.

Tolentino, P. L. M., R. D. Williams, and M. D. Hurst (2025). "Natural flood risk management in tropical Southeast Asia: prospects in the biodiverse archipelagic nation of the Philippines". In: *Wiley Interdisciplinary Reviews: Water* 12.1, e70000. URL: https://doi.org/10.1002/wat2.70000.

WISE Uranium Project (2025). *Chronology of major tailings dam failures*. Accessed: 2025-06-04. URL: https://www.wise-uranium.org/mdaf.html.

World Bank (2019). *Tailings Storage Facilities: Technical Note 7*. Tech. rep. Comprehensive guidance on TSF design, construction methods, and facility types. World Bank Group. URL: https://openknowledge.worldbank.org/bitstreams/b01ca405-ec83-5bd9-aef5-2f8e56a4767a/download.

Zhao, P., H. Xie, Q. Chen, X. Li, and S. Sun (2026). "A dual-path feature fusion model for tailings dam saturation line prediction driven by multi-source sensing data". In: *Measurement* 267, p. 120469. URL: https://doi.org/10.1016/j.measurement.2026.120469.

Zhen, Z., X. Ma, and B. Ma (2021). "Exploration and Research on the Propagation Law of Seepage Risk Network in Tailings Storage Facility". In: *Discrete Dynamics in Nature and Society* 2021.1, p. 8704259. URL: https://onlinelibrary.wiley.com/doi/abs/10.1155/2021/8704259.

Supplementary Files

This is a list of supplementary files associated with this preprint. Click to download.

- Modelscenarios.docx